A MAGNETIC EQUIVALENT CIRCUIT MODEL OF CONSEQUENT-POLE MAGNETIC SCREW BASED ON 2-D RELUCTANCE NETWORK

Shuangyu Chen[1], Lixun Zhu[1], Xinglong Jin[2], Zhixin Huang[1], Bo li[3], Xin Jin[3]

[1]Shanghai Maritime University, Shanghai, 201306, China
[2]Taiyuan Heavy Industry (Shanghai) Equipment Technology Co., Ltd, Shanghai, China
[3]Liaoning Inspection Examination and Certification Centre, Shenyang, 110031 China
202430210118@stu.shmtu.edu.cn

Keywords: MAGNETIC LEAD SCREW, CONSEQUENT POLE, MAGNETIC EQUIVALENT CIRCUIT, THRUST FORCE.

Abstract

In this paper, a two-dimensional (2-D) reluctance network magnetic equivalent circuit (MEC) model is proposed to reduce the performance analyzing time consumption at the design stage for the consequent-pole magnetic lead screw (CP-MLS). The solution region is desecrated by serious universality square grids, and each grid consists of four adjacent magnetic equivalent circuit cross-elements, which contain the reluctance and magnetomotive force along radial and axial directions. The flux of each branch in the model can be obtained after solving the combination equations from Kirchhoff's current equation of all the grids. Then the flux density and thrust force can be obtained. Finally, the effectiveness of the proposed MEC model is verified by the finite element method and experiment.

1 Introduction

Magnetic lead screw (MLS) is a magnetic force actuator that can convert linear and rotary motion into each other through the helical coupling magnetic field on the airgap between its mover and rotor. Compared with the mechanical screw, the MLS can avoid traditional mechanical contact, reduces friction and wear[1]-[2], and improves the service life and reliability of the system. Therefore, MLS has applications in many fields, such as energy harvesting, medical devices, aerospace actuation, etc[3]-[6]. A consequent-pole MLS(CP-MLS) is proposed to improve the utilization of permanent magnet (PM) of the traditional MLS, but its maximum thrust force will be decreased[7]. Therefore, a rapid analysis model for the CP-MLS is necessary to balance the performance between the utilization of PM and maximum thrust force at the optimal design stage.

At present, the analysis and optimization of MLS is mainly carried out by finite element method (FEM)[8], which provides accurate but time-consuming results[9]-[12]. The magnetic equivalent circuit (MEC) model has been paid attention to for accelerating the design process of the permanent magnetic machine because accurate results can be obtained, and the practice situation can be considered by parameterization. However, the model is complex and tedious because the MEC model corresponding to every instant time should be developed and its lumped parameters should be identified.

To simplify the modelling process, this paper proposes an MEC model to predict the transient trust force of the CP-MLS. In the proposed model, a uniform magnetic circuit mesh network is established through several basic magnetic circuit cross-elements. Both the radial and axis components of flux and PM exciting can be considered in each basic cross-element. After solving the Kirchhoff equations from each mesh establishes by four neighboring cross-element, the flux of each branch can be obtained. Then the magnetic density distribution and trust force can be calculated based on the flux of each cross-element. Finally, the proposed MEC model is verified by comparing the results with the FEM and experiment.

2. Topology and Operation Principle

2.1 Topology

The topology of the CP-MLS is shown in Fig. 1, it consists of two parts, the rotor, and the mover, Since the operating region of CP-MLS depends on the length of the rotor, this results in most of the PMs on the mover being inactive during MLS operation. To reduce the consumption of PMs, based on the traditional MLS, a consequent-pole structure is used on the mover, only one N-pole or S-pole is set to magnetically couple with the rotor, which is similar to the traditional consequent-pole PM machine[13], can reduce the consumption of PMs. The missing pole on the mover is replaced by teeth.

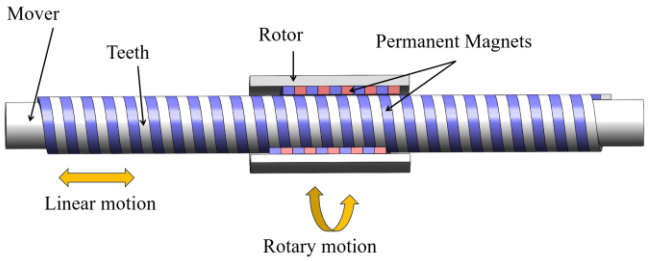

Fig. 1 Structure of the CP-MLS.

2.2 Operation Principle

The CP-MLS works on the same principle as traditional MLS. Through the helically coupled magnetic field in the air gap between the rotor and the prime mover, the thrust F of the mover can be transferred to the torque T of the rotor and vice versa.

The relationship between the speed of the mover v and the rotor speed ω follows:

$$v = \frac{\tau_p}{2\pi}\omega \tag{1}$$

where τ_p indicates the pitch of the MLS pole.

Neglecting the losses, according to the law of conservation of energy, the rotor's rotational output power is equal to the linear input power of the prime mover. The relationship between the prime mover thrust F and rotor torque T can be expressed as:

$$\tau_P F = \omega T \tag{2}$$

3. The Proposed Model

3.1 The Proposed MEC Model

The solution region of the proposed 2-D MEC model is located in the r-z (Radial-axis) plane as shown in Fig. 2. The proposed MEC model, which is further reduced to a pair of poles because of the periodicity of the CP-MLS in the z direction, is shown in Fig. 3. The solution area is divided by several square grid, which has the same length and height in the z and r directions throughout the model. Each grid is generated by four neighboring cross-elements.

The cross-elements located in the core, air gap, and PM region are shown in Fig.4, respectively. It contains four reluctances and two the magnetomotive force (MMF). The two axial reactance in the z-direction Rz1, Rz2 and two radial reactance in the r-direction Rz1, Rz2 can be calculated as:

$$R_{z1} = R_{z2} = l / \left[2u_0 u_r \pi \left(r_2^2 - r_1^2 \right) \right] \tag{3}$$

$$R_{r1} = R_{r2} = h / \left[2u_0 u_r \pi l \left(r_1 + r_2 \right) \right] \tag{4}$$

where l is the width of the grid, h is the height of the grid, r_1 is the inner radius of the grid, r_2 is the outer radius of the grid, μ0 is the vacuum permeability, and μ_r is the relative permeability of the grid.

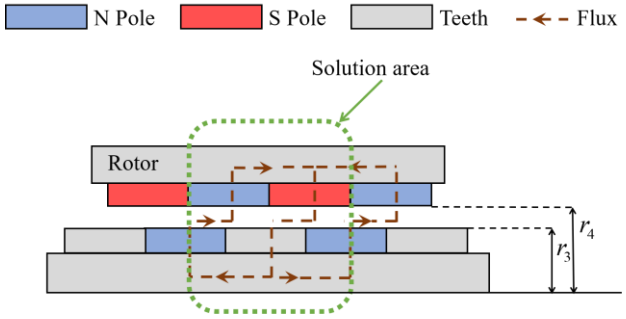

Fig. 2 The solution area of the proposed MEC model.

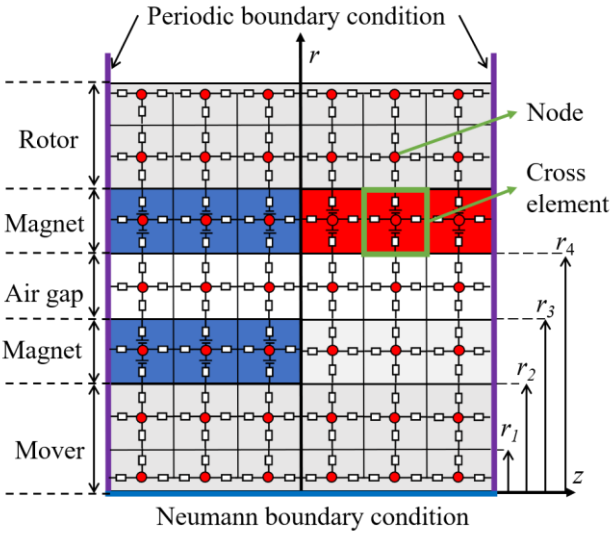

Fig. 3 The dicereted gird of the proposed MEC model.

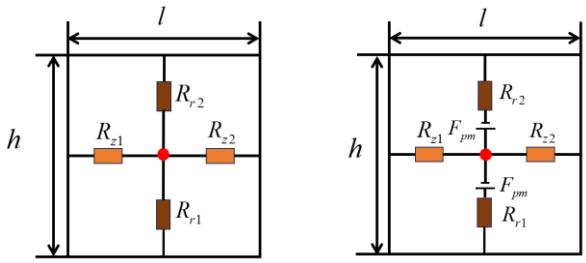

Fig. 4 Cross mesh element, (a) Core and air-gap parts, (b) PM part.

Because in the CP-MLS, the excitation source of the magnetic field is only PMs, and the permeability of PMs is constant. From this the magnetomotive force (MMF) in the MEC model can be expressed as:

$$F_{pm} = B_r h_{pm} / 2\left(\mu_0 \mu_{pm}\right) \tag{5}$$

where F_{pm} is the MMF of PM, Br is the residual amount of PM, μ_{pm} is the relative permeability of PM, and h_{pm} is the height of PM.

3.2 Numerical Calculation

After defining the magnetic flux Φ_i as the current circulating in the equivalent circuit, Kirchhoff's voltage law can be applied to the i^{th} grid shown in Fig. 5, the following equation can be obtained:

$$4F_{pm}=\left(R_{z_2}^{i}+R_{z_1}^{i+1}\right)\left(\Phi_i-\Phi_{i+m}\right)+\left(R_{r_1}^{i}+R_{r_2}^{i-m}\right)\left(\Phi_i-\Phi_{i-1}\right)$$
$$+\left(R_{z_2}^{i-m}+R_{z_1}^{i-m+1}\right)\left(\Phi_i-\Phi_{i-m}\right)+\left(R_{r_1}^{i+1}+R_{r_2}^{i-m+1}\right)\left(\Phi_i-\Phi_{i+1}\right) \quad (6)$$

where m denotes the quantity of the mesh elements in the z direction. Expanding equation (6) and replacing the coefficients in front of Φ_i and Φ_j with $R_{(i,i)}$ and $R_{(i,j)}$ transforms it into the form of equation (7):

$$R_{(i,i)}\Phi_i+R_{(i,i+m)}\Phi_{i+m}+R_{(i,i-1)}\Phi_{i-1}+R_{(i,i+1)}\Phi_{i+1}+R_{(i,i-m)}\Phi_{i-m}=4F_{pm}$$

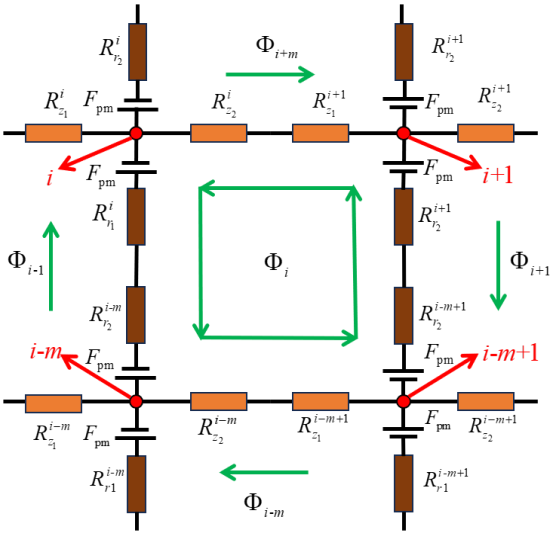

Fig. 5 The structure of the i^{th} grid.

Associate so the lattice circuits to obtain a non-chiral system of equations:

$$\begin{pmatrix} R_{(1,1)} & \cdots & R_{(1,n)} \\ \vdots & \ddots & \vdots \\ R_{(n,1)} & \cdots & R_{(n,n)} \end{pmatrix}\begin{pmatrix} \Phi_1 \\ \vdots \\ \Phi_n \end{pmatrix}=\begin{bmatrix} F_1 \\ \vdots \\ F_n \end{bmatrix} \quad (7)$$

where n represents the total amount of the mesh, $R(i,i)$ denotes the reluctance value contained in the i^{th} mesh, $R(i,j)$ denotes the reluctance value between the i^{th} mesh and the j^{th} mesh.

Since the matrix in (8) concerning the magnetoresistance is a sparse matrix with a large dimension, the successive over-relaxation (SOR) method is used to solve (8). The MMF, R, and Φ are related as follows:

$$\Phi_i^{k+1}=-\left\{\frac{\omega}{R}\left[\sum_{j=1}^{i-1}R_{(i,u)}\Phi_j^{(k+1)}-\sum_{u=1}^{n}R_{(i,j)}\Phi_j^{(k+1)}-F_i\right]-\Phi_i^k\right\} \quad (8)$$

To determine whether convergence has been achieved, the value of Φ_i^k subtracted from the Φ_i^{k+1} of the previous generation and the next generation is compared with the iterative error ζ. The accuracy error has the following expression:

$$\left|\Phi_i^{k+1}-\Phi_i^k\right|<\zeta \quad (9)$$

3.3 Flux Density and Thrust Force

The magnetic flux density B at the i^{th} node is given by:

$$B_{ir}=\frac{\Phi_{1r}}{2S_r}+\frac{\Phi_{2r}}{2S_r} \quad (10)$$

$$B_{iz}=\frac{\Phi_{1z}}{2S_z}+\frac{\Phi_{2z}}{2S_z} \quad (11)$$

where Sz is the axial cross-sectional area of the mesh element, and Sr is the radial cross-sectional area of the mesh element. And the reference direction of the flux as shown in Fig. 6.

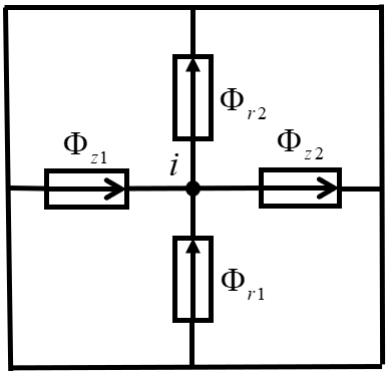

Fig. 6 Flux direction of the i^{th} grid

The thrust force generated by the solution region can be calculated as:

$$F=\frac{\pi r_a}{\mu_0}\int_0^{l_z}B_z\left(z,r_a\right)B_r\left(z,r_a\right)dz \quad (12)$$

$$r_a=\frac{r_3+r_4}{2} \quad (13)$$

where l_z is the distance that the mover moves in the axial direction relative to the rotor, r_a is the average radius of the air gap, $B_z(z,r_a)$ is the axial component of the magnetic density at the air gap r_a and $B_r(z,r_a)$ is the radial component of the magnetic density at the air gap r_a.

3.4 Implementation

The proposed model is implemented in Matlab.

Step.1: Determine the element numbers N_{sz} and N_{sr} along the z and r directions, respectively.

Step.2: Determine the motion step of the MEC model.

Step.3: Solve the equivalent reluctance and magnetic potential of each grid by (3) and (4).

Step.4: Calculate the voltage balance equation for each grid through (7).

Step.5: Solve (8) to get the flux of all the grids.

Step.6: Solve (13) and (14) for the thrust force of the mover at the relative position.

Step.7: Change the position of the mover and repeat steps 3-6 until all the steps have been calculated to solve for the thrust force.

4 Model Validation

In this paper, the 2-D as well as 3-D FEM models are constructed to verify the proposed MEC model. Also, the proposed MEC model is verified by experiment through a CP-MLS prototype. The specification of the prototype is shown in Table I and materials of each part of CP-MLS is shown in Table Ⅱ, which are also applied to the proposed MEC, 2-D, and 3-D FEM models.

4.1 Experimental Platform

The laboratory prototype and the corresponding test platform of the CP-MLS as shown in Fig. 7. In the test platform, the linear motor is used to drive the translator of the proposed CP-MLS, and the translator and rotor are supported by the linear slider and the bearing, respectively.

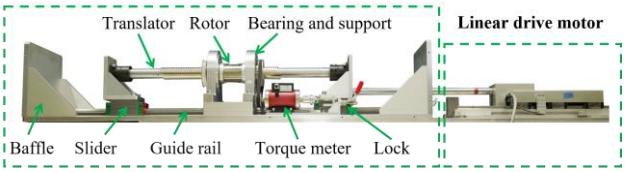

Fig. 7 A small-scale laboratory prototype and the corresponding test platform of the CP-MLS.

The helical PM pole on the rotor and mover consists of 8 spiral permanent magnet segments. To ensure installation accuracy, the PM segments are mounted by the bolt-on method, using threaded holes drilled in the permanent magnet segments and threaded holes drilled in the inner surface of the rotor to mount the permanent mag-net segments. The permanent magnet on the outer surface of the mover also consists of 8 segments of helical permanent magnets and 8 segments of helical teeth, which are mounted using threaded holes drilled in the segments and teeth and threaded holes drilled in the outer surface of the mover.

Table I The Specification of CP-MLS

Symbol	Parameters	Values
R_1	Outer radius of mover	22(mm)
R_2	Outer radius of mover PM	27(mm)
R_3	Inner radius of rotor PM	28(mm)
R_4	Outer radius of rotor PM	33(mm)
R_5	Outer radius of rotor	38.5(mm)
τ_s	Pole distance	10(mm)
B_r	Magnet remanence	1.2(T)
μ_0	Vacuum permeability	$4\pi\times10\text{-}7(\text{N}\cdot\text{A}^2)$
μ_r	Relative permeability	1.06

Table II Materials in Each Part Of CP-MLS

Object	Material
PM	NdFe35
Mover	Steel-1008
Rotor	Steel-1008
Teeth	Steel-1008

4.2 Verification Results

As the grid of the proposed MEC is divided smaller, the result will be more accurate. However, its influence is negligible and the speed of calculation is greatly affected. So set the length and width of the grid to 0.5mm to ensure the accuracy of the experimental results and the rapidity of the calculation.

MEC, 2-D FEM, and 3-D FEM to get the B contrast in both directions at r_a when the mover is half a pole pitch distance apart relative to the rotor is shown in Fig. 8. It can be seen from the figure that the results of MEC coincide with that of the 2-D and 3-D FEM well.

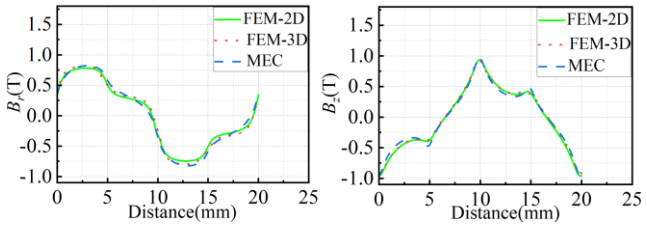

Fig. 8 The distribution of ***B*** comparisons by the MEC and 2-D FEM and 3-D FEM, (a) Radial division of ***B***. (b) Axial division of ***B***.

In Fig. 9(a), the experiment thrust force results are measured by moving the mover 20mm along the axial direction. The thrust force results among the pro-posed MEC, experiment, 2-D, and 3-D FEM results with their harmonic analysis are shown in Fig. 9(b). From Fig. 9, it can be seen that the thrust force of the pro-posed MEC is matched well with that of the experimental, 2-D, and 3-D FEM results. The time consumption comparison of 3-D FEM and MEC when displacement step is 1mm are 324 minutes and 16.49 seconds with the CPU i7-10710U (1.10 GHz), RAM 16 GB, respectively. It is show that the proposed MEC has great time advantage.

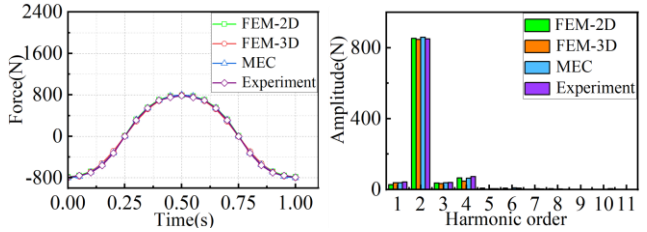

Fig. 9 Comparison of MEC with 2D FEM and 3D FEM transient analysis results, (a) Thrust curves;,(b) Harmonic analysis.

5 Conclusion

This paper proposes a 2-D magnetic equivalent circuit model to predict the performance of CP-MLS. A uniform magnetic circuit mesh network is established through several basic magnetic equivalent circuit cross-elements. Both the radial and axis components of flux and PM exciting can be considered in each basic cross-element. After solving the Kirchhoff equations from each mesh established by four neighboring cross-elements, the flux of each branch can be obtained. Then the magnetic density distribution and trust force can be calculated based on the flux of each cross-element. Finally, the B in the air gap and trust force results from the proposed MEC are compared with that of experimental, 2-D, and 3-D FEM results, and they are

matched well. The proposed MEC is also applicable to other types of magnetic helices and more complex structures.

6 References

[1] Holm, R.K., Berg, N.I., Walkusch, M., et al.: 'Design of a Magnetic Lead Screw for Wave Energy Conversion', Ieee Transactions on Industry Applications, 2013, 49, (6), pp. 2699-2708

[2] Li, L., and Zhu, G.J.: 'Electromagnetic-Thermal-Stress Efforts of Stator-Casing Grease Buffers for Permanent Magnet Driving Motors', Ieee Transactions on Industry Applications, 2024, 60, (1), pp. 1268-1276

[3] Lu, K.Y., and Wu, W.M.: 'Electromagnetic Lead Screw for Potential Wave Energy Application', Ieee Transactions on Magnetics, 2014, 50, (11)

[4] Meng, S.J., Ling, Z.J., Zhao, et al.: 'Design and Analysis of a Surface-Inserted Magnetic Screw With Minimum Thrust Force Ripple', Ieee Transactions on Transportation Electrification, 2024, 10, (4), pp. 9406-9415

[5] Zhu, L.X., Ma, C., Li, W., et al.: 'A Novel Hybrid Excitation Magnetic Lead Screw and Its Transient Sub-Domain Analytical Model for Wave Energy Conversion', Ieee Transactions on Energy Conversion, 2024, 39, (3), pp. 1726-1737

[6] Ji, J.H., Ling, Z.J., Wang, J.B., et al.: 'Design and Analysis of a Halbach Magnetized Magnetic Screw for Artificial Heart', Ieee Transactions on Magnetics, 2015, 51, (11)

[7] Zhu, L.X., Wu, Q.Y., Li, W., et al.: 'A Novel Consequent-Pole Magnetic Lead Screw and its 3-D Analytical Model With Experimental Verification for Wave Energy Conversion', Ieee Transactions on Energy Conversion, 2024, 39, (2), pp. 1202-1215

[8] Gao, F., Wang, Q., Zou, J.B., et al.: 'Development of Equivalent 2-D Finite-Element Models for Accurate Prediction of Thrust Force in Permanent Magnet Lead Screws', Ieee Transactions on Magnetics, 2017, 53, (11)

[9] Jin, P., Tian, Y., Lu, Y., et al.: '3-D Analytical Magnetic Field Analysis of the Eddy Current Coupling With Halbach Magnets', Ieee Transactions on Magnetics, 2020, 56, (1)

[10] Song, J.Y., Lee, J.H., Kim, et al.: 'Analysis and Modeling of Concentrated Winding Variable Flux Memory Motor Using Magnetic Equivalent Circuit Method', Ieee Transactions on Magnetics, 2017, 53, (6)

[11] Sun, X.D., Xu, N.X., et al.: 'Sequential Subspace Optimization Design of a Dual Three-Phase Permanent Magnet Synchronous Hub Motor Based on NSGA III', Ieee Transactions on Transportation Electrification, 2023, 9, (1), pp. 622-630

[12] Gao, F., Wang, Q., and Zou, J.B.: 'Analytical Modeling of 3-D Magnetic Field and Performance in Magnetic Lead Screws Accounting for Magnetization Pattern', Ieee Transactions on Industrial Electronics, 2020, 67, (6), pp. 4785-4796

[13] Wang, K., Li, F., Sun, H.Y., et al.: 'Consequent Pole Permanent Magnet Machine With Modular Stator', Ieee Transactions on Vehicular Technology, 2020, 69, (7), pp. 7054-7063